Biomaterials 30 (2009) 8–18

Contents lists available at ScienceDirect

Biomaterials

journal homepage: www.elsevier.com/locate/biomaterials

The effect of organo clay and adsorbed FeO_3 nanoparticles on cells cultured on Ethylene Vinyl Acetate substrates and fibers

Hilana M. Lewkowitz-Shpuntoff [a,*], Mary C. Wen [b], Avtar Singh [c], Nicole Brenner [d], Richard Gambino [d], Nadine Pernodet [d], Rebecca Isseroff [e], Miriam Rafailovich [d,*], Jon Sokolov [d]

[a] Department of Chemistry, Princeton University, Princeton, NJ 08544, USA
[b] Department Electrical Engineering, Princeton University, Princeton, NJ 08544, USA
[c] Department of Physics, Cornell University, Ithaca, NY 14850, USA
[d] Department of Material Science and Engineering, SUNY at Stony Brook, Stony Brook, NY 11794, USA
[e] Lawrence High School, Cedarhurst, NY 11516, USA

ARTICLE INFO

Article history:
Received 28 June 2008
Accepted 2 September 2008
Available online 5 October 2008

Keywords:
Elastomer
Nanocomposite
Fibroblast
Osteoblast
Cell proliferation
Electrospun fibers

ABSTRACT

Nanocomposites of Ethylene Vinyl Acetate (EVA 260) with Cloisite 20A organo clay and Cloisite 20A organo clay impregnated with $Fe(CO)_5$ were produced in a twin-screw extruder. Dynamic mechanical analysis (DMA) measurements indicated that the moduli increased monotonically for the Cloisite, up to a concentration of 10%, after which the modulus decreased. Adult human dermal fibroblasts (AHDF) were plated on these surfaces and the cell growth was found to be maximal on the nanocomposites containing 10% Cloisite. AHDFs cultured on substrates with higher Cloisite content had low surface area, poor growth curves, and misshaped actin fibers. Compounding EVA with $Fe(CO)_5$ soaked Cloisite did not enhance the modulus even at a loading of 10%. TEM images indicate nanoparticles form and coat the Cloisite platelet surfaces, possibly interfering with the exfoliation process. On the other hand, cell culture of MC3T3 osteoblasts proliferated on the Fe containing nanocomposites, the largest effect being observed when cultured in a constant magnetic field. These results indicate how the chemical nature of the Cloisite 20A organo clay can also play a major role. Finally, since natural ECM is fibrillar, these EVA nanocomposites were also electrospun into micron thick fibers. MC3T3s proliferated well on these fibers and the MC3T3 proliferation was maximized by culture on electrospun aligned fibers in a constant magnetic field.

© 2008 Elsevier Ltd. All rights reserved.

1. Introduction

Nanoparticles have become the catalyst behind many novel technologies mainly because of their large surface-to-volume ratio. However, there is concern about the potential long-term harmful effects of their use. For example, even nanoparticles that consist of biologically inert materials can harm cells by penetrating the cell membrane, disrupting intracellular processes [1–4] and attaching to DNA [5]. Nanoparticles are commonly blended with polymers to form nanocomposites. Clays, which are composed of platelets that have a thickness on the order of 1 nm, and range from 8 to 10 μm in diameter, are a frequent component of nanocomposites [6–10]. Due to their high aspect ratio, clays increase the strength, mechanical modulus, and toughness of the polymer while also improving barrier and flame retardant properties [11]. Furthermore, some clays have been shown to contain Fe, Na, and other minerals, and hence exhibit either charge or magnetic properties.

As a result, clay nanocomposites are currently being used in numerous applications which range from electronics and reinforcing structural materials, to viscosity modifiers in personal care products and controlling the gas/bio-organism permeability of biomedical plastics [12,13]. Yet despite their popularity and ubiquitous use, little is known regarding their interactions with living tissues and cells. We therefore decided to focus on this aspect of clay nanocomposites. We first performed studies of cell morphology and proliferation as a function of clay concentration. We then modified the clays by exposing them to Fe pentacarbonyl vapors, which penetrated the galleries and rendered the clays magnetic. Hence magnetic polymer nanocomposites could be molded from these clays, and the effects of external magnetic fields could be studied. Previous research has shown that strong magnetic fields can stimulate bone growth [14–19]. Hence for these studies we chose to use osteoblasts, and probe the effect of the external fields on their proliferation and orientation. Since the skin is also the first point of contact with nanoparticles that are encased, we also tested the effects of clay nanocomposites on primary culture dermal fibroblast cells.

* Corresponding authors.
E-mail address: hlewkowi@princeton.edu (H.M. Lewkowitz-Shpuntoff).

0142-9612/$ – see front matter © 2008 Elsevier Ltd. All rights reserved.
doi:10.1016/j.biomaterials.2008.09.015

We first experimented with flat surfaces, but since the actual ECM formed by the dermal fibroblasts in vivo is fibrillar [20–22], we also had electrospun fibers of the nanocomposites, and studied the effects of the fibrillar structures. In this study we chose to use Ethylene Vinyl Acetate random copolymers (EVA 260) because it is an elastomer whose modulus more closely resembles tissue than that of hard glassy polymers.

2. Materials and methods

2.1. Preparation of bulk nanocomposite samples

2.1.1. Preparation of magnetic clay platelets

Five grams of Cloisite 20A (Southern Clay Products, Gonzales, TX) organo clay was placed in a glass jar and sealed with a rubber stopper. $Fe(CO)_5$ (Aldrich, St. Louis, MO) liquid was then injected through the stopper, such that the clay and Fe carbonyl were in a 1:1 ratio by mass, or 5 g Cloisite to 3.4 mL $Fe(CO)_5$. The powder was then stirred for 5 min and left sealed in the glass jar overnight. The following morning, the powder was stirred again for 5 min and then the mixture was left under a ventilated hood for 24 h. During that time all $Fe(CO)_5$ liquid was adsorbed within the clay galleries and allowed to decompose. Some of the platelets were then encased in a glassy polymethylmethacrylate (PMMA) matrix and microtomed at room temperature. The micrographs are shown in Fig. 1, where we can see that the $Fe(CO)_5$ decomposed to form nanoparticles which appear to be adsorbed to the clay platelets. Additionally, as shown in Fig. 1(A), there is an even distribution and exfoliation of the Cloisite 20A platelets throughout the polymer matrix. Furthermore, in Fig. 1(B) the Fe-nanoparticles are clustered along the exfoliated clay platelets. The average size of the particles obtained is 3.5 nm. Another set of samples was also made where the amount of the $Fe(CO)_5$ was doubled and was added in a 1:2 ratio (5 g Cloisite, to 6.7 mL $Fe(CO)_5$). The amount of Fe in each of the samples containing $Fe(CO)_5$ was determined using mass spectroscopy at Desert Analytics, Inc., in Tucson, AZ.

2.1.2. Polymer nanocomposite blending

The polymer we used was EVA 260 (DuPont Corp, Wilmington, DE), which is a rubbery polymer at room temperature with $T_m = 75\,^{\circ}C$. The nanocomposites were blended in a Brabender (C.W. Brabender Instruments, Inc., South Hackensack, NJ) by using the following procedure:

The total mass of EVA 260 and nanoparticles in all of the nanocomposites produced was 50 g. First, half of the mass of EVA 260 was poured into the Brabender which was rotating at 5 revolutions per minute at 150 °C. When all of the EVA 260 that was poured in was molten, half of the mass of the nanoparticles was added into the Brabender. When it appeared that all of the nanoparticles have been incorporated into the polymer matrix, half of the remaining EVA 260 was added and when all of the EVA 260 that had been added was molten, half of the remaining nanoparticles were added into the Brabender. When it appeared that all of the nanoparticles had been incorporated into the polymer matrix, the remaining EVA 260 was added into the Brabender; when the EVA 260 that was just added in was in a molten state, the remaining nanoparticles were added into the brabender. The brabender was closed and the rotation speed was increased to 100 revolutions per minute for 20 min at 150 °C to ensure homogeneity. The brabending process was carried out to produce the nanocomposites that consisted of 95% EVA with 5% Cloisite 20A, 92% EVA 260 with 8% Cloisite 20A, 90% EVA 260 with 10% Cloisite 20A, 88% EVA 260 with 12% Cloisite 20A, 85% EVA 260 with 15% Cloisite 20A, 80% EVA 260 with 20% Cloisite 20A, 80% EVA 260 with 20% Cloisite 20A:$Fe(CO)_5$ in a 1:1 ratio, 90% EVA 260 with 10% Cloisite 20A:$Fe(CO)_5$ in a 1:1 ratio, and 90% EVA 260 with 10% Cloisite 20A:$Fe(CO)_5$ in a 1:2 ratio.

2.1.3. Preparation of bulk nanocomposite samples

The nanocomposites were molded into disks 1.5 cm in diameter using a Carver Heated Press (Carver, Inc., Wabash, IN). The bulk samples were pressed between Kapton polyimide films (DuPont Corp, Wilmington, DE) in order to keep the roughness below 100 nm. 100% EVA 260 was also pressed into bulk disks for cell growth tests. The pure polymer and the nanocomposites were adhered to 24-well dishes (Becton Dickinson Labware, Franklin Lakes, NJ) by adding three drops of toluene (Fisher Scientific Company, Pittsburgh, PA) beneath the disks, which temporarily plasticizes the polymer, but evaporated quickly, so that they would not float in the cell media. The surfaces were sterilized for cell plating under an ultraviolet light lamp (Englehard Industries, Inc., Newark, NJ) for 30 min.

2.1.4. Preparation of electrospun nanocomposite samples

Electrospinning is a process that creates a mat of fibers using an electric charge. A viscous polymer solution is drawn into a syringe, and then a high voltage supply is attached to the needle. A graduated pump slowly and uniformly pushes the solution out of the needle, and the high voltage stretches the solution droplet into a Taylor cone and an electrified jet is formed. The jet is continuously elongated by electrostatic charge repulsion and solvent evaporation, creating a mat of electrospun fibers on the grounded collector surface.

1.40 grams of 100% EVA 260, 90% EVA with 10% Cloisite 20A, and 90% EVA 260 with 10% Cloisite 20A:$Fe(CO)_5$ in a 1:2 ratio by mass were each added to four vials, each containing 8.6 mL of chloroform (J.T. Baker, Phillipsburg, NJ), to create a 14% w/v solution. The solutions were left for 24 h on a 100 °C surface to completely dissolve the pure polymer and the nanocomposites. 3 mL of the dissolved solution were drawn into a 5 mL glass syringe (Hamilton Company, Reno, NV) that was then secured onto the graduated pump (Kd Scientific, Holliston, MA), and the flow rate was set to 3 mL/h. The high voltage power supply (Gamma High Voltage Research, Ormond Beach, FL) was set to 10 kV and attached to the needle, and the collector surface was grounded. The fibers were collected on approximately .75 cm^2 silicone wafer chips (Umicore Semiconductor Processing, Boston, MA) to make the mesh nanofiber surfaces. To create the aligned fibers, wafer chips were attached to a cylindrical rotator (Talboys Engineering, Thorofare, NJ). The electrospinning set up was the same as was used to create the mesh fibers, with the addition of the cylindrical rotator, which was set at 700 rotations per minute. When the fibers landed on the surface, they were immediately pulled straight by the rotations and aligned onto the silicon wafer. The electrospun mesh and the electrospun aligned fibers were examined with a light microscope (Olympus, Center Valley, PA) at 100× magnification. The average size of the fibers obtained was 7.1 μm and 7 μm with and without clay. The addition of clay therefore did not change the fiber diameter significantly. The spacing between the fibers was 15.1 μm. All the electrospun samples were sterilized with the ultraviolet lamp for 30 min.

2.2. Characterization of clay polymer nanocomposite substrates

2.2.1. Vibrating sample magnetometry

A Vibrating Sample Magnetometer (VSM) (Digital Measuring Systems, Westwood, MA) measured the magnetic moment of iron oxide in all of the samples. Using

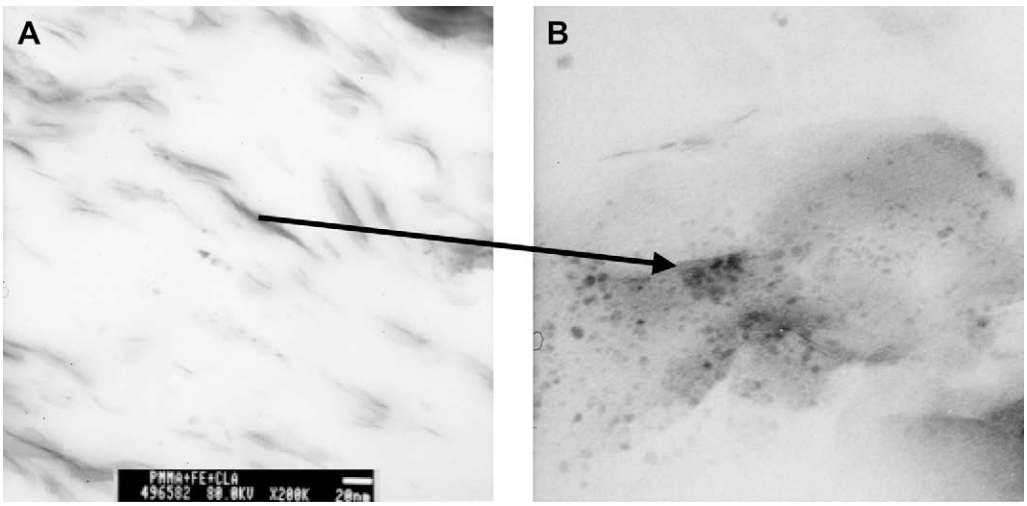

Fig. 1. Micrographs of the $Fe(CO)_5$ – Cloisite 20A platelets encased in PMMA: (A) Cloisite 20A platelets are exfoliated and distributed evenly throughout the polymer matrix (B) Fe-nanoparticles are clustered along the exfoliated clay platelets.

rubber cement, the sample is attached to a vertically vibrating glass rod suspended between a pair of magnetic coils, and the flux changes caused by the movement of the sample introduce a current in the coils, which is read by an ammeter.

Paramagnetic samples have a strong affinity to external magnetic fields but lose all magnetism once the field is removed. A hysteresis loop resulting from the VSM will show a straight, positive slope in the presence of paramagnetic nanocomposites. Diamagnetic samples have a negative slope and no magnetic properties. To calculate the magnetism of each sample, the measured magnetization, measured in memu was divided by the fractional iron content, as determined from mass analysis.

2.2.2. Dynamic mechanical analysis

Dynamic mechanical analysis (Triton Technology, Ltd., Keyworth, Nottinghamshire, UK) was performed to determine the effects of clay/Fe on the mechanical properties of the materials. The nanocomposites studied were as follows: 100% EVA 260, 92% EVA 260 with 8% Cloisite 20A, 90% EVA 260 with 10% Cloisite 20A, 88% EVA with 12% Cloisite 20A, 90% EVA 260 with 10% Cloisite 20A:$Fe(CO)_5$ in a 1:1 ratio, and 90% EVA 260 with 10% Cloisite 20A:$Fe(CO)_5$ in a 1:2 ratio. The samples for the DMA tests were molded at 150 °C for 10 min at 7 metric tons in the heat press to fit the DMA's dimensions, which were approximately 2 mm × 10.5 mm × 11 mm. When mounted in the DMA, the samples were heated from room temperature to 160 °C at a rate of 2 °C per minute. An oscillating force was applied to the sample, and the displacement of the sample was recorded. The modulus, a measure of stiffness, was then calculated from the stress over the strain.

2.3. Cell culture

Adult Human Dermal Fibroblasts (AHDF), CF-31, were obtained from Clonetics, San Diego, CA. The adult human dermal fibroblasts were cultured in DMEM supplemented with 10% fetal bovine serum (HyClone, Logan, UT) and an antibiotic mix of Penicillin–Streptomycin. MC3T3 osteoblasts were obtained from ATCC and routinely cultured in Minimum Essential Medium α (Gibco, Grand Island, NY) containing 10% Fetal Bovine Serum (HyClone, Logan, UT) and 1% Penicillin–Streptomycin (Gibco, Grand Island, NY). All cells were cultured in a 37° C, 5% CO_2 95% humidity incubator (Napco Scientific Company, Tualtin, OR).

2.4. Cell proliferation

Passage 2 AHDFs were plated on the bulk polymer-clay nanocomposites consisting of EVA and different concentrations of clay at 2.0×10^3 cells per cm^2 and incubated for 4 days in a 37° C, 5% CO_2 95% humidity incubator (Napco Scientific Company, Tualtin, OR). Four surfaces per condition were selected per day for 10 days. The surfaces were rinsed twice with PBS, and then 200 μL of trypsin was added to each well and incubated for 1 min. 400 μL of media was then added to each well to neutralize the trypsin and by using a hemocytomer, the number of cells per surface were calculated for each of the different clay polymer nanocomposite surfaces. Passage 2 MC3T3 osteoblasts were plated on the bulk and electrospun clay nanocomposites consisting of EVA and $Fe(CO)_5$ at 2.4×10^3 cells per cm^2 and incubated for 4 days under the same incubation conditions as the AHDFs. One group of plated surfaces was set as the control, and the other group was exposed to a magnetic field. To create the magnetic field, a 24-well dish containing the nanocomposites was sandwiched between two layers of Neodymium magnets (Max Magnetic Products, Flushing, NY). Four surfaces per condition were selected after 4 days. The surfaces were rinsed twice with PBS, and then 400 μL of trypsin was added to each well and incubated for 10 min. 400 μL of media was then added to each well to neutralize the trypsin and by using a hemocytomer, the number of cells per surface were calculated for each of the different clay polymer nanocomposite surfaces. In this configuration, the magnetic field at the center of the cell culture dish was measured using a Hall probe and found to be 1.5 KG.

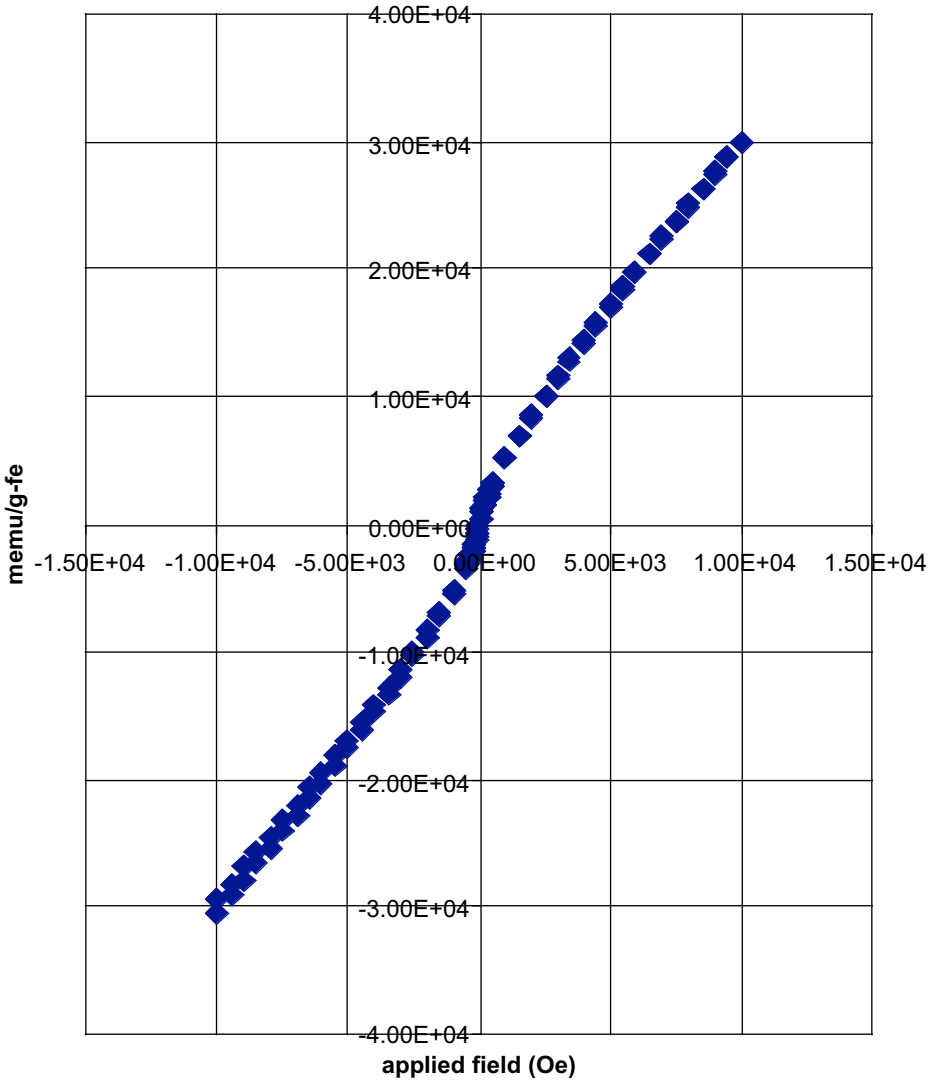

Fig. 2. Magnetic moment due to Fe in the 80% EVA 20% Cloisite 20A:$Fe(CO)_5$ 1:1.

2.5. Cell morphology and orientation

Passage 2 AHDFs were seeded on clay polymer nanocomposites consisting of EVA 260 and different concentrations of clay at 2.0×10^3 cells per cm^2 and incubated for 4 days in a 37° C, 5% CO_2 95% humidity incubator (Napco Scientific Company, Tualtin, OR). The MC3T3s were seeded on the bulk and electrospun clay polymer nanocomposites with different ratios of $Fe(CO)_5$ at 2.4×10^3 cells per cm^2 and incubated for 4 days in magnetic and non magnetic fields. The choice of this incubation time was based on the observation that both the AHDFs and the MC3T3s on the different surfaces showed significant differences in rates of proliferation after 4 days.

To determine actin cytoskeleton organization of the dermal fibroblasts, and the orientation of the osteoblasts, the cells were fixed with 3.7% (w/v) formaldehyde for 15 min and then washed twice with PBS. Next the cells were permeabilized with a mild detergent (1% Nonidet P-40, Sigma) for 10 min, and then stained with a 1:100 dilution of Alexa Fluor-488 Phalloidin (Molecular Probes, Eugene, OR) to 2% Bovine Serum Albumin (BSA) (Sigma-Aldrich, St. Louis, MO) in PBS for 20 min. The surfaces were rinsed and stored in 1 mL of PBS. The cells were then imaged using a Leica TCS SP2 laser scanning confocal microscope (Leica microsystem Inc., Bannockburn, IL).

2.6. Data analysis

Data is expressed as mean +/− standard deviation and evaluated for differences by Student's *t*-Test. Differences were considered significant when $p < .05$.

3. Results and discussion

3.1. Magnetic nanocomposite characterization

In order to determine the effects of magnetic substrates on cell properties we first characterized the magnetic properties of the substrates by using a VSM to measure the magnetic moment of iron oxide in all of the samples. VSM detected superparamagnetic properties for the nanocomposites containing iron and Cloisite. Fig. 2 shows the magnetic properties of the 80% EVA 260 with 20% Cloisite 20A:$Fe(CO)_5$ in a 1:1 ratio due solely to the iron present in the sample. As shown in Fig. 2, the sample exhibits superparamagnetism, as indicated by the positive slope and lack of hysteresis. Clustered iron oxide nanoparticles inhibit the expression of magnetism; however because the exfoliation of the Cloisite 20A nanoparticles distributes the iron oxide nanoparticles, the nanocomposites are capable of having paramagnetic properties. The zero field intercept (spontaneous magnetization) is 2.5 emu/g Fe for 80% EVA 260 with 20% Cloisite 20A:$Fe(CO)_5$ in a 1:1 ratio, .021 emu/g Fe for the 90% EVA 260 with 10% Cloisite 20A:$Fe(CO)_5$ in a 1:1 ratio (Fig. 3) and .087 emu/g Fe for the 90% EVA 260 with 10% Cloisite 20A:$Fe(CO)_5$ in a 1:2 ratio (Fig. 4). These very small magnitudes of magnetization suggest that the samples consist of nanoscale αFe_2O_3, which is an antiferromagnet. The other samples did not exhibit ferromagnetic properties and thus, the emu/g could not be calculated.

3.2. Dynamic mechanical analysis

Because the modulus of the surface also affects the function of cells cultured on the nanocomposites, DMA was performed to determine the effects of clay/Fe on the mechanical properties of the materials. The moduli of the nanocomposites with EVA are plotted in Fig. 5 as a function of Cloisite concentration. From the figure we find that the moduli increase monotonically with increasing Cloisite content, up to a concentration of 10%, where an enhancement of 228% over the unfilled systems is observed. Addition of more Cloisite, however is seen to decrease the modulus. As the percentage of Cloisite is increased passed 10%, the degree of exfoliation is decreased and tactoids begin to form as the Cloisite platelets become increasingly confined. This results in a decrease in modulus since the tactoids interfere with the gel – like state which is formed when the Cloisite platelets exfoliate to a large degree in a polymer matrix above Tg.

Adding Cloisite to the nanocomposites where Fe carbonyl was adsorbed onto the surfaces, forming clay nanoparticles, is seen to reduce the modulus even further for the 10% blends. Here we postulate that the Fe particles coating the Cloisite platelet surfaces screens the favorable interactions between the EVA and the functionalized clays, thereby eliminating the enhanced reinforcement of the mechanical properties and the analogously large moduli observed.

3.3. Cell proliferation and adhesion on bulk EVA clay nanocomposites

We first wanted to determine the effects of addition of the organo clays to EVA polymers. We therefore cultured AHDFs from primary culture on the molded EVA samples with different amounts of added Cloisite 20A organo clay. The control sample was plated on a glass cover slip. The cell proliferation over 4 days of incubation is shown in Fig. 6. Cell proliferation on all of the surfaces increased minimally by day 1. However this is expected because the average doubling time for AHDFs is approximately 20 h. By day 3 cell counts on the 100% EVA substrates were significantly lower than those on the glass control sample ($p = .0073$), indicating that EVA is not a good substrate for these cells. The addition of 5% Cloisite 20A to the EVA polymer matrix significantly improved cell viability in comparison to the 100% EVA substrate ($p = .0229$). A maximum improvement was observed with the addition of 10% Cloisite 20A. The difference between the amount of cell proliferation with the addition of 5% Cloisite 20A and the amount of cell proliferation with the addition of 10% Cloisite 20A by day 3 was also significant ($p = .013$). Additionally, the 90% EVA 260 with 10% Cloisite 20A substrates even supported more cell proliferation than was seen on the glass control ($p = .0429$). However, further addition of clay of 15% and 20% decreases the cell count. The 85% EVA 260 with 15% Cloisite 20A supported significantly less cell proliferation ($p = .011$). These same trends continued on day 4. Figs. 7 and 8 are low and high magnification confocal microscope images of the cells on these substrates taken using a Leica TCS SP2 laser scanning confocal microscope (Leica microsystem Inc., Bannockburn, IL). At 4 days the cells are observed to be confluent on the glass control substrate, forming a tissue.

On the 100% EVA substrates, from the higher magnification image we observe that the cell area is smaller than on the control, and that the cell's actin fibers are not well developed. The cell appears to have an abnormal morphology, in which it is lacking the defined structure as seen in the AHDFs plated on the glass control. Many more cells are observed on the substrates with added 5% and 10% Cloisite 20A in comparison to the cells plated on the 100% EVA surfaces. Here multi layers of tissue have formed after 4 days and the density is much higher than on the glass control. Higher magnification images show that the cells are well spread with well formed actin fibers. Addition of more clay, 15% and 20%, has an obvious deleterious effect on the cells. The cell density is clearly much lower, and the cell area is smaller. Thus, addition of up to 10% Cloisite 20A organo clay in the polymer matrix had a dramatic beneficial effect on cell proliferation and morphology.

Cells may detect and respond to mechanical cues, which are increasingly being understood to play a role in cell adhesion response. Numerous studies have found that physical and chemical properties of the adhesion substrate can affect cell locomotion, growth, and differentiation [23–25]. Cells respond to differences in substrate flexibility by altering their adhesion structures, often translated through their actin organization, and mobile behavior. In a study by Wang et al. [26], surface flexibility was controlled by varying the concentration of the cross linkers bisacrylamid in acrylamide. Cells were found to proliferate better on more rigid substrates. The cells on the rigid substrate were well spread out, indicating a good adhesion and healthy cell, and appeared identical to cells cultured on glass or plastic surfaces. However, the cells that were plated on the more flexible substrates showed a change in morphology, smaller in size and with a poor adhesion. It has also

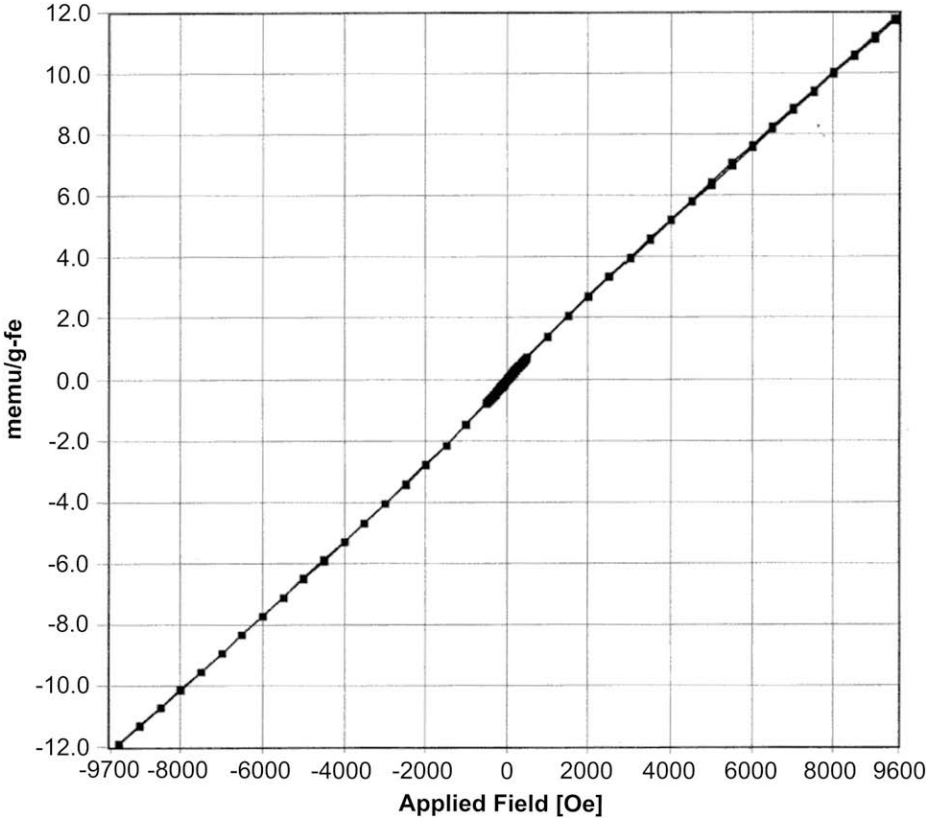

Fig. 3. Magnetic moment due to Fe in the 90% EVA 260 with 10% Cloisite 20A:$Fe(CO)_5$ in a 1:1 ratio.

been reported that cells preferentially migrate toward hard surfaces, which provide traction for cells [27].

We therefore suggest that the increased cell number and the improved morphology of the cells on the substrates containing 10% Cloisite are due to the larger modulus measured by DMA. As the Cloisite concentration increases past 10%, the modulus of the nanocomposite drops and there is greater chance of excess free surfactant blooming to the surfaces. This has an adverse effect on the

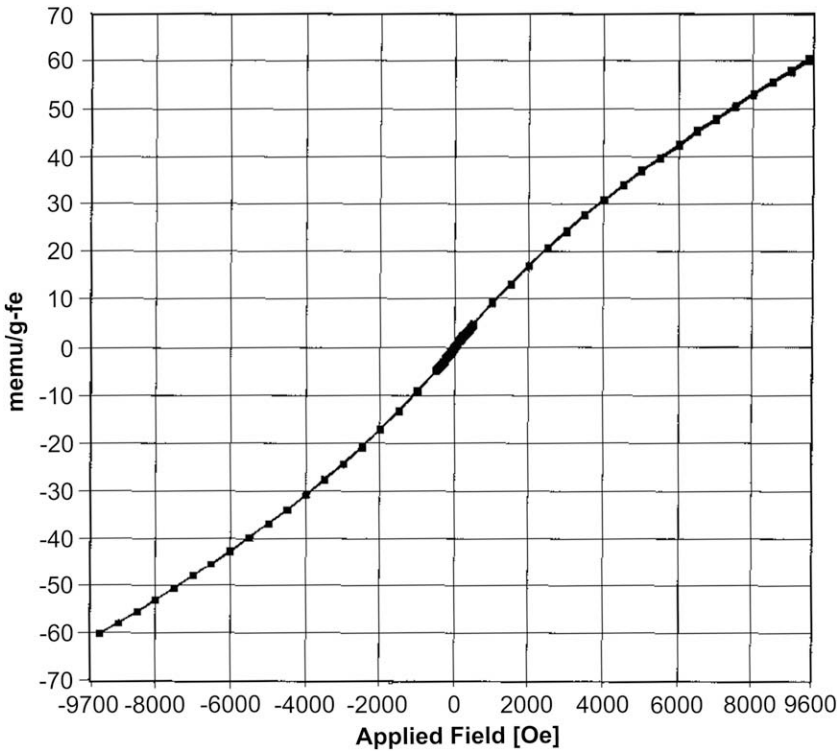

Fig. 4. Magnetic Moment due to Fe in the 90% EVA 260 with 10% Cloisite 20A:$Fe(CO)_5$ in a 1:2 ratio.

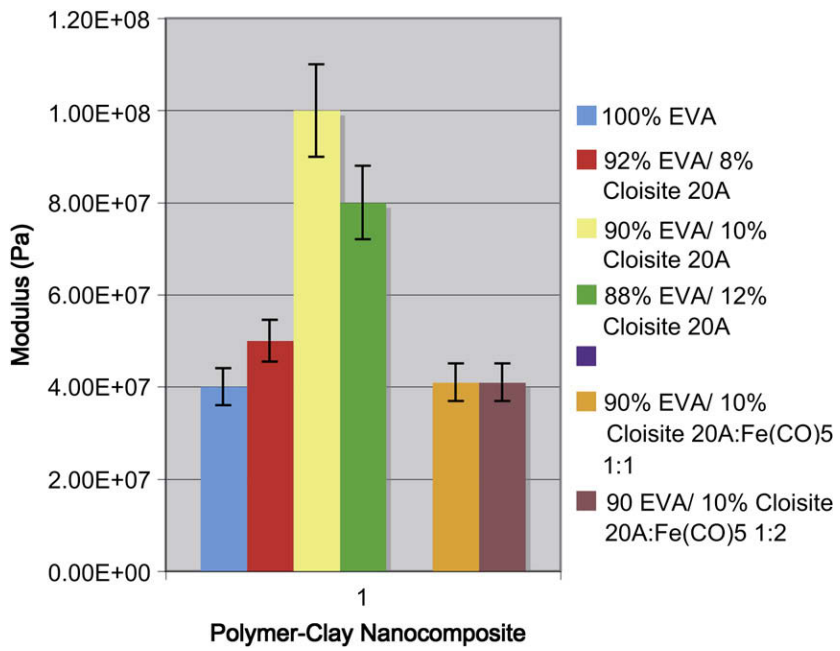

Fig. 5. Room temperature moduli of EVA/Cloisite 20A clay nanocomposites: the right most data points correspond to EVA with 20A Cloisite clays which had adsorbed $Fe(CO)_5$.

cells, as can be seen in the significantly lower cell counts and the confocal images shown. Because we observe a maximum of cell proliferation at 10% Cloisite 20A, which corresponds to the largest modulus observed within the EVA polymer-clay nanocomposites indicates that surface mechanics is an important parameter governing cell viability.

3.4. Osteoblast proliferation and orientation on EVA clay nanocomposites with the addition of Fe_2O_3

Since bone cells are known to be sensitive to magnetic fields, Passage 2 MC3T3 osteoblasts were plated on the bulk and electrospun clay nanocomposites consisting of EVA and $Fe(CO)_5$ at 2.4×10^3 cells per cm^2 and incubated in magnetic and non magnetic fields for 4 days under the same incubation conditions as the AHDFs. After 4 days the cells were counted and a graph depicting the cell density on each of the nanocomposite surfaces in magnetic and non magnetic fields relative to the cell density on the glass control in magnetic and non magnetic fields respectively were constructed (Fig. 9).

Data is not available for the number of cells per surface on the electrospun mesh and aligned fibers for 100% EVA 260 because due to the soft nature of EVA, the mats peeled off the silicon wafers after the second culture day during feeding. For cell proliferation on the bulk disks without magnetic fields, both the 90% EVA 260 with 10% Cloisite 20A and the 90% EVA 260 with 10% Cloisite 20A:$Fe(CO)_5$ 1:2 nanocomposites significantly increased cell proliferation compared

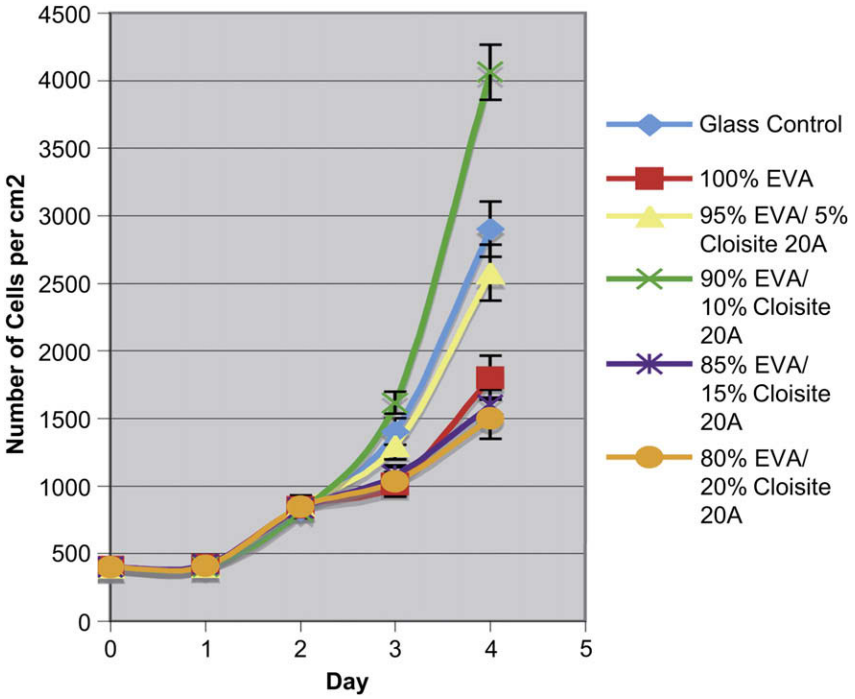

Fig. 6. Proliferation of AHDFs on EVA/Cloisite 20A clay nanocomposites over 4 days of incubation.

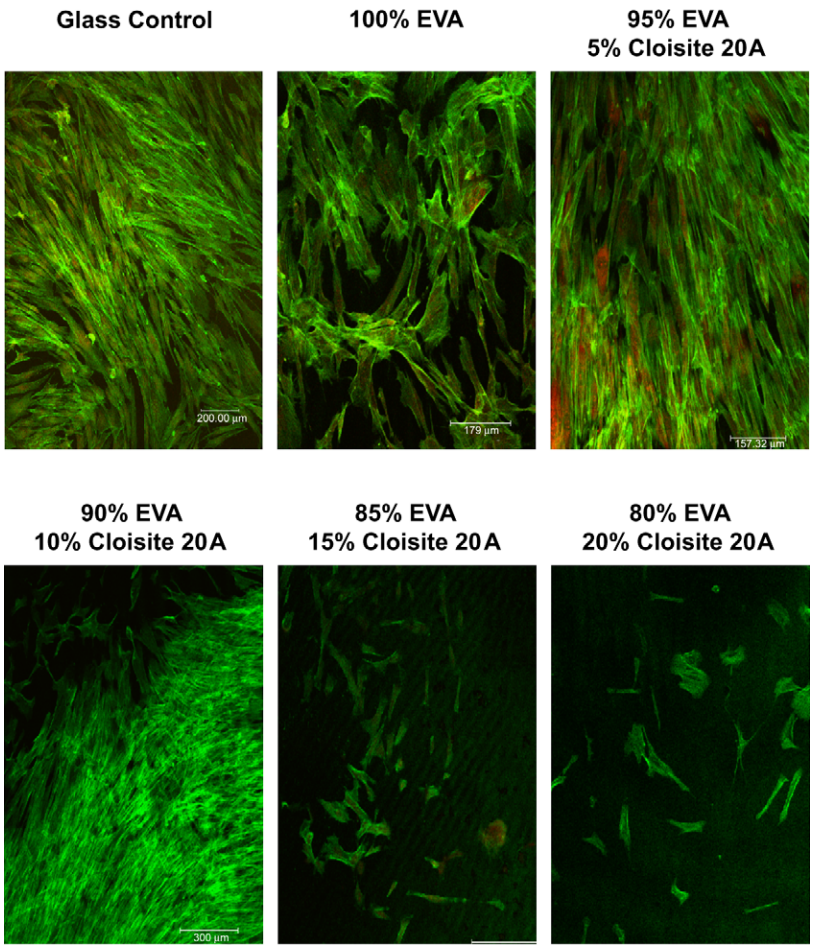

Fig. 7. AHDFs on EVA/Cloisite 20A clay nanocomposites after 4 days of incubation at 10× magnification.

to the pure polymer with p values of .0002 and .0001 respectively (Fig. 9). However, there was not a significant difference between the amount of cell proliferation on the 90% EVA 260 with 10% Cloisite 20A bulk surfaces and the 90% EVA 260 with 10% Cloisite 20A:$Fe(CO)_5$ in a 1:2 ratio bulk surfaces.

In comparison to the proliferation on the bulk nanocomposites, the proliferation of the cells plated on the electrospun mesh fibers was greater. Specifically the 90% EVA 260 with 10% Cloisite 20A electrospun meshed fibers supported greater cell proliferation than the 90% EVA 260 with 10% Cloisite 20A bulk surface ($p = .0001$). Additionally, the 90% EVA 260 with 10% Cloisite 20A:$Fe(CO)_5$ in a 1:2 ratio meshed fibers also supported greater cell proliferation than the 90% EVA 260 with 10% Cloisite 20A:$Fe(CO)_5$ in a 1:2 ratio bulk surface ($p = .0006$). The electrospun aligned fibers generated the greatest amount of cell proliferation within the three surface types (Fig. 9). Specifically the 90% EVA 260 with 10% Cloisite 20A electrospun aligned fibers supported greater cell proliferation than the 90% EVA 260 with 10% Cloisite 20A meshed fiber surfaces ($p = .0012$). The 90% EVA 260 with 10% Cloisite 20A:$Fe(CO)_5$ in a 1:2 ratio aligned fibers also supported greater cell proliferation than the 90% EVA 260 with 10% Cloisite 20A:$Fe(CO)_5$ in a 1:2 ratio meshed fibers ($p = .0003$). The addition of the magnetic field enhanced cell proliferation for all materials and surface types (Fig. 9). When cultured in a magnetic field, the 90% EVA 260 with 10% Cloisite 20A:$Fe(CO)_5$ in a 1:2 ratio again experienced the greatest amount of cell proliferation for the three types of surfaces, with the highest cell density on the electrospun aligned fibers. Additionally, there was no significant difference in cell proliferation on 90% EVA 260 with 10% organo clay: $Fe(CO)_5$ 1:2 electrospun aligned fibers with and without magnetic fields.

Images of the MC3T3s on these substrates were taken using a Leica TCS SP2 laser scanning confocal microscope (Leica microsystem Inc., Bannockburn, IL). Fig. 10(A) shows MC3T3 proliferation and organization of those cells plated on bulk disks consisting of 90% EVA 260 with 10% Cloisite without the presence of external magnets. The presence of an external magnetic field on the cell growth on the of 90% EVA 260 with 10% Cloisite bulk disks enhanced cell proliferation and communication as indicated by the presence of filapodia (Fig. 10B). With the addition of Fe_2O_3 to the EVA clay substrate, it seems that the MC3T3 proliferation was further enhanced (Fig. 10C). Additionally, the cells are organized in a circular formation, which corresponds to the direction of the magnetic flux. Within the last 10 years, research has indicated that Ca^{2+} plays a critical role in cell signaling through classical intracellular mechanisms. Additionally Ca^{2+} serves as an extracellular or "first" messenger [28–33]. We postulate that because the Ca^{2+} ions orient in the direction of the magnetic flux, and that Ca^{2+} is crucial in cell signaling, that the cells themselves also orient in the direction of the magnetic flux. Thus the circular formation of the cells on the Fe/Cloisite nanocomposite surfaces in the presence of the magnetic field, in the direction of the magnetic flux indicates that the external magnetic field plays a large role in tissue formation via cellular organization using ion exchange in filapodia.

Prior research has indicated that strong magnetic fields of tesla order can regulate and orient matrix proteins and cells [34–43].

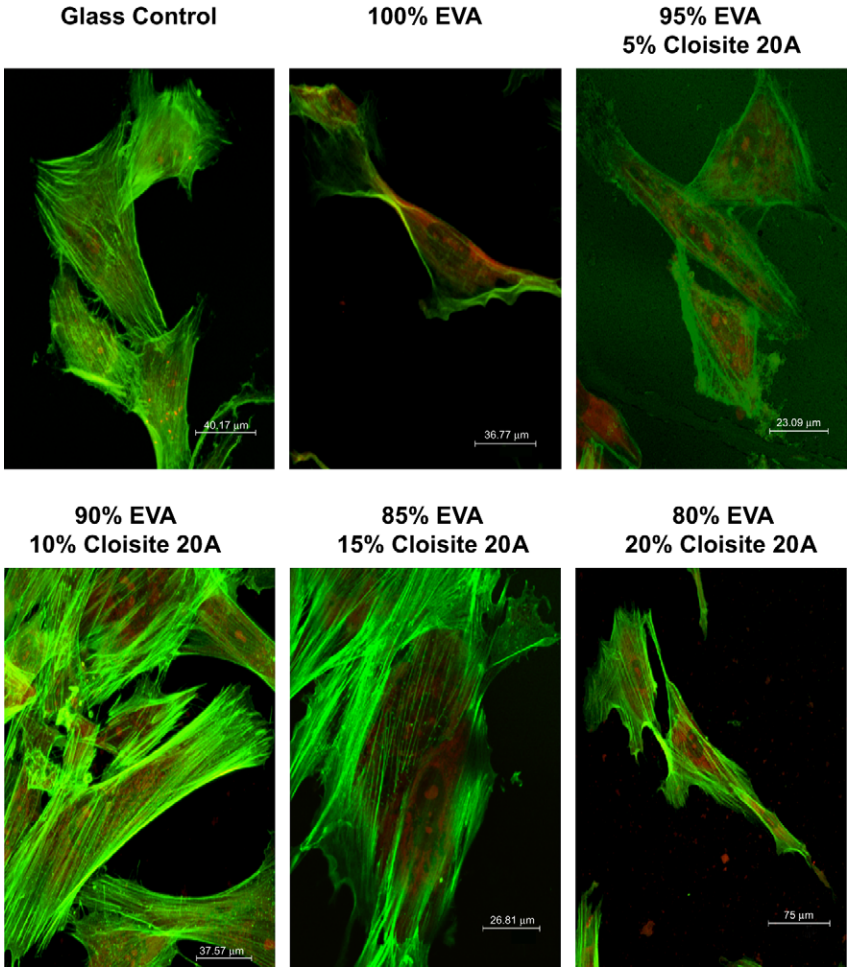

Fig. 8. AHDFs on EVA/Cloisite 20A clay nanocomposites after 4 days of Incubation at 40× magnification.

Under SMF of 5–10 T, matrix proteins are orientated to a regular pattern. These oriented proteins then facilitate the orientation of cells. However, right now the mechanism is not fully understood. In this study the fields are much smaller, but they may be enough to induce orientation.

Confocal images of the MC3T3s on electrospun mesh surfaces all indicate healthy cell growth with stretched actin fibers adhering to the substrate. Images of cells on 90% EVA 260 with 10% Cloisite 20A:$Fe(CO)_5$ in a 1:2 ratio (see Fig. 11(B,D) and Fig. 12(B,D)) show denser growth in comparison to cells on 90% EVA 260 with 10%

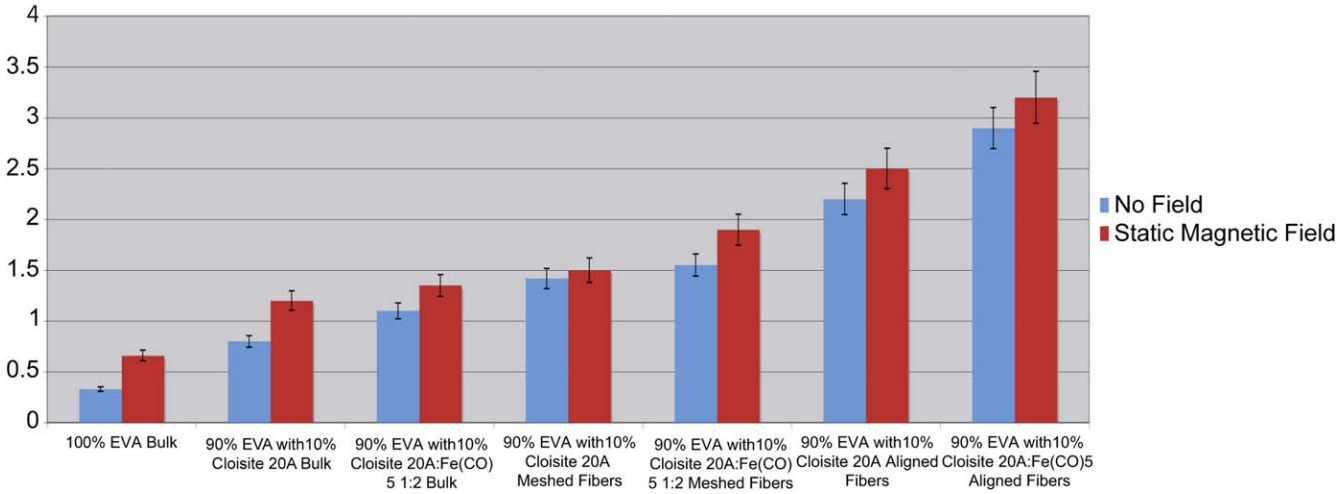

Fig. 9. Ratio of the density of MC3T3s on each nanocomposite surface to the density of MC3T3s on the glass control after 4 days of incubation in magnetic and non magnetic Fields.

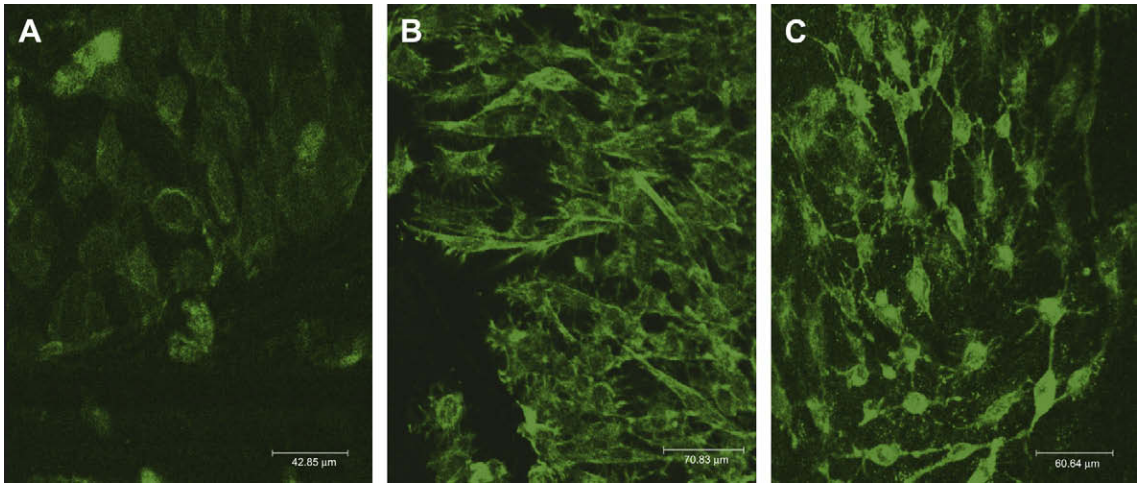

Fig. 10. MC3T3s plated on bulk nanocomposite surfaces after 4 days of incubation in magnetic and non magnetic fields at 20× magnification: (A) MC3T3's plated on 90% EVA 260 with 10% Cloisite 20A and incubated without magnetic Field (B) MC3T3's plated on 90% EVA 260 with 10% Cloisite 20A and incubated in the presence of a static magnetic field (C) MC3T3s plated on 90% EVA 260 with 10% Cloisite 20A:$Fe(CO)_5$ 1:2 and incubated in the presence of a static magnetic field; MC3T3s are organized in a circular formation corresponding to the direction of the magnetic flux.

Cloisite (Fig. 11(A,C) and Fig. 12(A,C)), which correlates with the cell counts (Fig. 9).

MC3T3s on the electrospun aligned surfaces (Fig. 12) are much more prolific than the electrospun mesh surfaces (Fig. 11). This corresponds with the data from Fig. 9, which depicted the cell viability on electrospun surfaces. MC3T3s are adapting well to the configuration of the surface, and the stretched actin indicates that the cells are healthy and well-adhered to the surfaces. It is interesting to note that unlike the MC3T3s plated on the EVA 20A:$Fe(CO)_5$ in a 1:2 ratio bulk samples cultured in a magnetic field, the MC3T3s on the electrospun meshed and aligned fibers cultured in the magnetic field were not organized in a circular formation. This indicates that on the electrospun substrates, the magnetic field did not really control their alignment, but rather the configuration of the substrate dictated the orientation. The cells were so strongly oriented on the fibers that they ignored the external magnetic field. The MC3T3s cultured in a magnetic field on electrospun aligned fibers of 90% EVA 260 with 10% Cloisite 20A:$Fe(CO)_5$ in a 1:2 ratio had

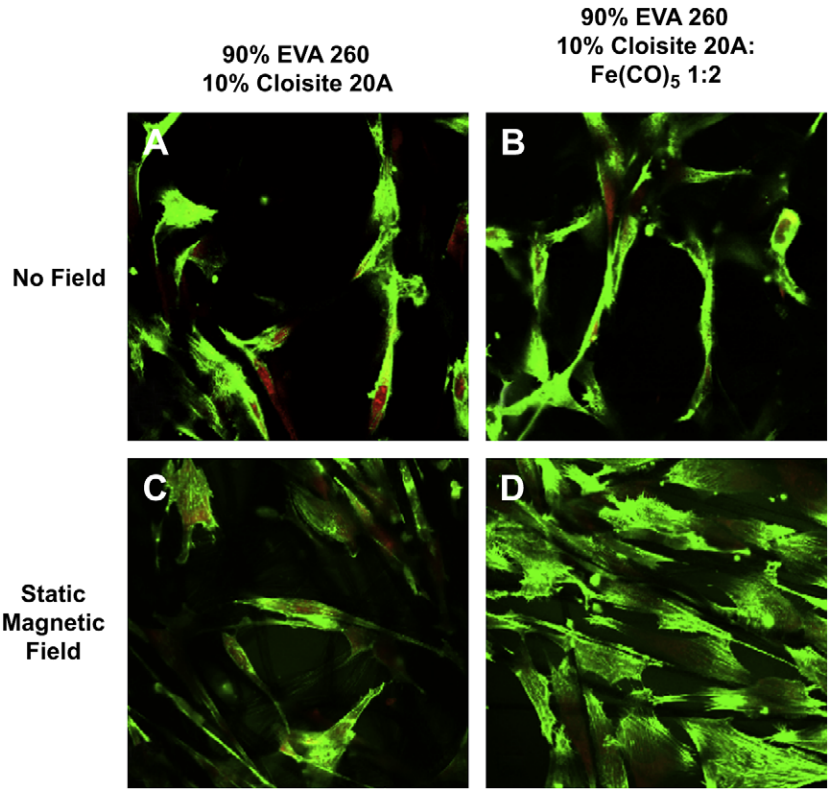

Fig. 11. MC3T3s on electrospun mesh fibers after 4 days of incubation at 63× magnification: (A) 90% EVA 260 with 10% Cloisite 20A with no field (B) 90% EVA 260 with 10% Cloisite 20A:$Fe(CO)_5$ 1:2 with no field (C) 90% EVA 260 with 10% Cloisite 20A cultured in a static magnetic field (D) 90% EVA 260 with 10% Cloisite 20A:$Fe(CO)_5$ 1:2 cultured in a static magnetic field.

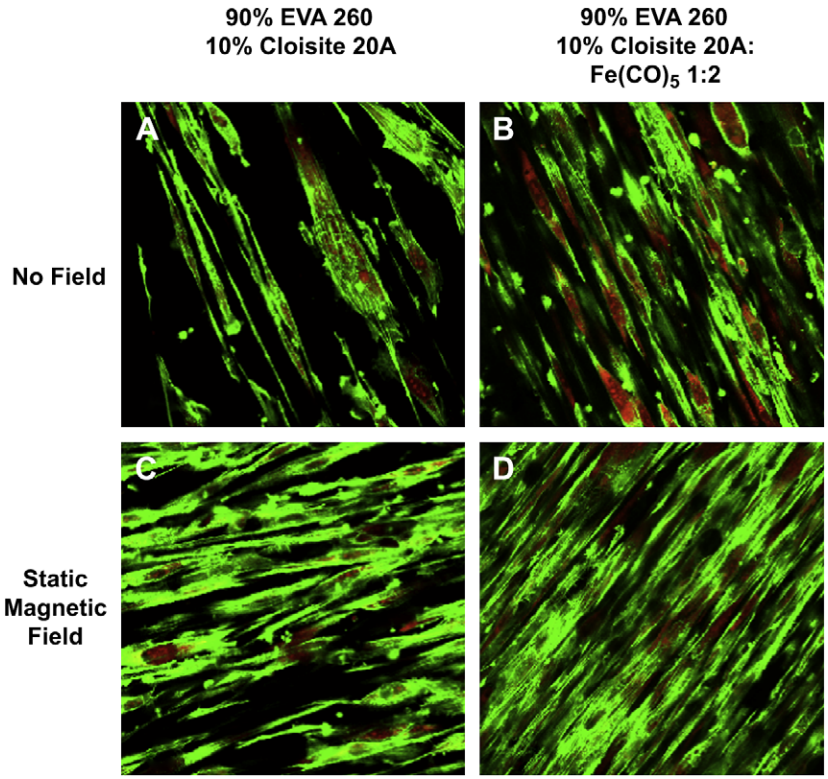

Fig. 12. MC3T3s on electrospun aligned fibers after 4 days of incubation at 63× magnification: (A) 90% EVA 260 with 10% Cloisite 20A with no field (B) 90% EVA 260 with 10% Cloisite 20A:$Fe(CO)_5$ 1:2 with no field (C) 90% EVA 260 with 10% Cloisite 20A cultured in a static magnetic field (D) 90% EVA 260 with 10% Cloisite 20A:$Fe(CO)_5$ 1:2 cultured in a static magnetic field.

the highest proliferation after the fourth day, and as depicted in Fig. 10. The cells are also confluent on the surface.

4. Conclusion

The addition of up to 10% Cloisite 20A to EVA 260 has a dramatic beneficial effect on cell proliferation and morphology. By placing Fe in the polymer through the adsorption to Cloisite, we successfully created a magnetic nanocomposite that enhanced the proliferation and alignment of MC3T3s when cultured in a magnetic field. The addition of Fe to the polymer-clay nanocomposites alone did not have a dramatic effect on proliferation. We saw that the largest effect on MC3T3s growth came from the presence of the static magnetic field. MC3T3 growth was maximized by seeding on electrospun aligned fibers consisting of 90% EVA with 10% Cloisite 20A:$Fe(CO)_5$ in a 1:2 ratio in a magnetic field. The presence of Fe increases the internal field near the cells and produces organization based on aligning the cells perpendicular to the field similar to the current flux in an external field. However when the MC3T3s are plated on electrospun aligned fibers, they strongly oriented on the fibers and ignored the external magnetic field.

Acknowledgements

This work was supported by the NSF-MRSEC program.

Appendix

Figures with essential colour discrimination. Certain figures in this article, particularly Figs. 7, 8, and 10–12, are difficult to interpret in black and white. The full colour images can be found in the on-line version, at doi: 10.1016/j.biomaterials.2008.09.015.

References

[1] Ophus EM, Rode LE, Gylseth B, Nicholson G, Saeed K. Analysis of titanium pigments in human lung tissue. Scand J Work Environ Health 1979;5:290–6.
[2] Lindenschmidt RC, Driscoll KE, Perkins MA, Higgins JM, Mourer JK, Belfiore KA. The comparison of a fibrogenic and two nonfibrogenic dusts by bronchoalveolar lavage. Toxicol Appl Pharmacol 1990;102(2):268–81.
[3] Oberdorster G, Ferin J, Lehnert BE. Correlation between particle size, in vivo particle persistence and lung injury. Environ Health Perspect 1994;102(5):173–9.
[4] Pernodet N, Fang X, Sun Y, Bakhtina A, Ramakrishnan A, Sokolov J, et al. Adverse effects of citrate/gold nanoparticles on human dermal fibroblasts. Small 2006;2(6):766–73.
[5] Tsoli M, Kuhn H, Brandau W, Esche H, Schmid G. Cellular uptake and toxicity of Au_{55} clusters. Small 2005;1(8–9):841–4.
[6] Giannelis EP. Polymer-layered silicate nanocomposites: synthesis, properties and applications. Appl Organomet Chem 1998;12(10–11):675–80.
[7] LeBaron PC, Wang Z, Pinnavala TJ. Polymer-layered silicate nanocomposites: an overview. Appl Clay Sci 1999;15(1–2):11–29.
[8] Garcés JM, Moll DJ, Bicerano J, Fibiger RF, McLeod DG. Polymeric nanocomposites for automotive applications. Adv Mater 2000;12:1835–9.
[9] Alexandre M, Dubois P. Polymer-layered silicate nanocomposites: preparation, properties and uses of a new class of materials. Mater Sci Eng 2000;28(1–2):1–63.
[10] Ray SS, Okamoto M. Polymer/layered silicate nanocomposites: a review from preparation to processing. Prog Polym Sci 2003;28(11):1539–641.
[11] Hunter DL, Kamena KW, Paul DR. Processing and properties of polymers modified by clays. MRS Bull 2007 April;32:323–7.
[12] Chen GX, Yoon JS. Clay functionalization and organization for delamination of the silicate tactoids in poly(L-lactide) matrix. Macromol Rapid Commun 2005;26(11):899–904.
[13] Loizou E, Butler PD, Porcar L, Talmon Y, Kesselman E, Schmidt G. Large scale structures in nanocomposite hydrogels. Macromolecules 2005;38:2047–9.
[14] Qu C, Qin QH, Kang Y. A hypothetical mechanism of bone remodeling and modeling under electromagnetic loads. Biomaterials 2006;27(21):4050–7.
[15] Gjelsvik A. Bone remodeling and piezoelectricity-I. J Biomech 1973;6:69–77.
[16] Gjelsvik A. Bone remodeling and piezoelectricity-II. J Biomech 1973;6:187–97.
[17] Bessett CA, Valdes MG, Hernandez E. Modification of fracture repair with selected pulsing electromagnetic fields. J Bone Joint Surg 1982;64(6):888–95.
[18] McLeod KJ, Rubin CT. The effect of low frequency electrical field on osteogenesis. J Bone Joint Surg 1992;74(6):920–9.
[19] Giodano N, Battisti E, Geraci S, Fortunato M, Santacroce C, Rigato M, et al. Effect of electromagnetic fields on bone mineral density and biochemical markers of bone turnover in osteoporosis: a single-blind, randomized pilot study. Curr Ther Res Clin Exp 2001;62(3):187–93.

[20] Han D, Gouma P. Electrospun bioscaffolds that mimic the topology of extracellular matrix. Nanomedicine 2006;2(1):37–41.
[21] Li C, Vepari C, Jin HJ, Kim HJ, Kaplan DL. Electrospun silk-BMP-2 scaffolds for bone tissue engineering. Biomaterials 2006;27(16):3115–24.
[22] Lannutti J, Reneker D, Ma T, Tomasko D, Farson D. Electrospinning for tissue engineering scaffolds. Mater Sci Eng 2007;27(3):504–9.
[23] Li G, Joshi V, White RL, Wang SX, Kemp J, Webb C, et al. Detection of single micron-sized magnetic bead and magnetic nanoparticles using spin valve sensors for biological applications. J Appl Phys 2003;93(10):7557–9.
[24] Harris A. Behavior of cultured cells on substrata of variable adhesiveness. Exp Cell Res 1973;77(1):285–97.
[25] Pelham RJ, Wang YL. Cell locomotion and focal adhesions are regulated by substrate flexibility. Proc Natl Acad Sci U S A 1997;94:13661–5.
[26] Lo CM, Wang HB, Dembo M, Wang YL. Cell movement is guided by the rigidity of the substrate. Biophys J 2000;79:144–52.
[27] Folkman J, Moscona A. Role of cell shape in growth control. Nature 1978; 273:345–9.
[28] Brown EM, MacLeod RJ. Extracellular calcium sensing and extracellular calcium signaling. Physiol Rev 2001;81:239–97.
[29] Brown E, Pollak M, Seidman C, Seidman JG, Chou YHW, Riccardi D, et al. Calcium-ion-sensing cell-surface receptors. E N Engl J Med 1995;333(4):234–40.
[30] Zaidi M, Alam ASMT, Huang CL-H, Pazianas M, Bax CMR, Bax BE, et al. Extracellular Ca^{2+} sensing by the osteoclast. Cell Calcium 1993;14(4):271–7.
[31] Zaidi M, Adebanjo OA, Moonga BS, Sun L, Huang CL. Emerging insights into the role of calcium ions in osteoclast regulation. J Bone Miner Res 1999;14(5): 669–74.
[32] Berridge MJ. Inositol trisphosphate and calcium signalling. Nature 1993; 361(6140):315–25.
[33] Meissner G. Ryanodine receptor/Ca^{2+} release channels and their regulation by endogenous effectors. Annu Rev Physiol 1994;56:485–508.
[34] Torbet J, Ronziere M. Magnetic alignment of collagen during self-assembly. Biochem J 1984;219:1057–9.
[35] Murthy NS. Liquid crystallinity in collagen solutions and magnetic orientation of collagen fibrils. Biopolymers 1984;23(7):1261–7.
[36] Torbet J, Freyssinet JM, Hudry-Clergeon G. Oriented fibrin gels formed by polymerization in strong magnetic fields. Nature 1981;289:91–3.
[37] Ueno S, Iwasaka M, Tsuda H. Effects of magnetic fields on fibrin polymerization and fibrinolysis. IEEE Trans Magn 1993;29(6):3352–4.
[38] Iwasaka M, Ueno S, Tsuda H. Effects of magnetic fields on fibrinolysis. J Appl Phys 1994;75:105–7.
[39] Yamagishi A, Takeuchi T, Higashi T, Date M. Diamagnetic orientation of blood cells in high magnetic field. Physica B 1992;177(1-4):523–6.
[40] Higashi T, Yamagishi A, Takeuchi T, Kawaguchi N, Sagawa S, Onishi S, et al. Orientation of erythrocytes in a strong static magnetic field. Blood 1993;82(4): 1328–34.
[41] Higashi T, Yamagishi A, Takeuchi T, Date M. Effects of static magnetic fields on erythrocyte rheology. Bioelectrochem Bioenerg 1995;36(2):101–8.
[42] Higashi T, Sagawa S, Kawaguchi N, Yamagishi A. Effects of a strong static magnetic field on blood platelets. Platelets 1993;4:341–2.
[43] Vassilev PM, Dronzine RT, Vassileva MP, Georgiev GA. Parallel assays of microtubules formed in electric and magnetic fields. Biosci Rep 1982;2: 1025–9.